
CORROSION AND PROTECTION
OF METALS

Tribological Characteristics and Corrosion Resistance of Coatings Obtained by Electrospark Alloying, Pulsed Cathodic Arc Evaporation, and Hybrid Technology Using TiCNiCr and TiCNiCr–Dy₂O₃ Electrodes

A. D. Sytchenko^{a, *}, A. N. Sheveyko^{a, **}, E. A. Levashov^{a, ***}, and Ph. V. Kiryukhantsev-Korneev^{a, ****}

^aNational University of Science and Technology “MISIS”, Moscow, Russia

*e-mail: alina-sytchenko@yandex.ru

**e-mail: sheveyko@mail.ru

***e-mail: levashov@shs.misis.ru

****e-mail: kiruhancev-korneev@yandex.ru

Received December 12, 2019; revised January 17, 2020; accepted January 21, 2020

Abstract—Single- and double-layer coatings on 40Cr steel substrates have been obtained by electrospark alloying (ESA) and a combination of ESA technology and pulsed cathodic arc evaporation (PCAЕ) using TiCNiCr and TiCNiCr–Dy₂O₃ electrodes. The electrodes are obtained by powder metallurgy. The structure and elemental and phase composition of the electrodes and coatings are studied using scanning electron microscopy, energy dispersive spectroscopy, and X-ray phase analysis. The tribological properties of the coatings are determined as a result of tests according to the pin-on-disk scheme in contact with the Al₂O₃ counterbody at loads of 1, 5, and 10 N. The temperature during the tests is $T = 20^{\circ}\text{C}$. The potential and current density of corrosion are determined using a three-electrode cell with a VoltaLab 50 potentiostat. The results show that the electrodes consist of TiC grains of 12 μm ; a solid solution of Ni in Cr; and, in the case of a doped electrode, Dy₂O₃ up to 5 μm in size. ESA coatings have a low-defect fine-grained structure consisting of regions of a solid solution of Ni and Cr in Fe and titanium carbide grains with a maximum size of 0.3 μm . Coatings with the addition of Dy₂O₃ have a lower coefficient of friction at loads of 1, 5, and 10 N. All coatings in 1 N H₂SO₄ are in a stable passive state and have high corrosion resistance: the corrosion current density of the coatings is at least 4 times lower than the values obtained for a 40Cr steel substrate.

Keywords: TiC, NiCr, Dy₂O₃, electrospark alloying, pulsed cathodic arc evaporation, coatings, friction coefficient, current density of corrosion

DOI: 10.3103/S1067821220030177

INTRODUCTION

In the field of creating protective coatings that increase the wear, heat, and corrosion resistance of products, the development of tungsten-free hard alloys based on TiC is a promising direction [1, 2]. They consist of a solid phase TiC surrounded by a metal binder (Ni). In such materials, carbide grains provide high mechanical properties and a nickel matrix improves strength characteristics and corrosion resistance [3–5]. The additional introduction of chromium into the composite material increases the mechanical and tribological characteristics, as well as the heat resistance of the coatings [6]. The introduction of 1–2% of borides into the composition of TiC–Ni electrodes improves the physicochemical parameters of the doped layer, reduces its roughness, and increases its wear resistance [7].

It is important to note that the addition of ceramic nanoparticles to the composition of electrode materials leads to a modification of their structure and an increase in hardness (by 20%) and crack resistance (by 40%) [8], which is important for increasing the service life of electrodes. Doping TiC-based coatings with rare-earth metals and their oxides makes it possible to modify the structure, reduce the friction coefficient, and increase the mechanical properties of coatings [9, 10].

We previously showed that the introduction of Eu₂O₃ to the composition of TiCNiCr electrodes makes it possible to increase their strength characteristics [11], the growth rate of coatings [12], and their mechanical and tribological properties of coatings [13]. In this work, the concentrations of chromium and nickel were increased (4 times) when compared

Table 1. Composition of powders for the manufacture of electrodes

Electrode	Content, at %			
	TiC	Ni	Cr	Dy ₂ O ₃
TiCNiCr	50	16.7	33.3	–
TiCNiCr–Dy ₂ O ₃	50	16.3	32.7	1.0

with previous studies. Pulsed cathode-arc evaporation [12] using these electrodes, first proposed in [14], is promising for coating.

Dysprosium oxide is widely used as optical layers [15, 16], as well as anticorrosion coatings [17]. There are known cases of positive effects of Dy₂O₃ on the tribological properties of coatings. The authors of [18] attribute this to the fact that the Dy₂O₃ particles in the tribocontact zone serve as a solid lubricant, which helps reduce the friction coefficient and increase the wear resistance of coatings.

The aim of this work was to obtain coatings obtained by TiCNiCr and TiCNiCr–Dy₂O₃ electrodes using the technology of electrospark alloying (ESA), as well as study the effect of deposition of the upper layer by pulsed arc evaporation (PCAE) on the structure and properties of electrospark coatings.

MATERIALS AND METHODS

Powders were used as the initial components for the manufacture of electrodes; their composition is given in Table 1.

The powders were mixed in an Activator-2S planetary centrifugal mill in an argon atmosphere for 5 min and pressed on a hydraulic press at pressure 200 MPa. The resulting briquettes 5 × 5 × 42 mm and 10 × 10 × 75 mm in size were sintered in a filling with Al₂O₃ in a VE-3-16 vacuum furnace (LLC NPP VakETO, Russia) at a temperature of 1450°C for 60 min. Polished steel disks of brand 40Cr (analogue to steel 5140) with a size of Ø30 × 5 mm were used as substrates. Before coating, the substrates were sonicated in C₃H₈O for 5 min on a UZDN-2T installation.

The coatings were applied using an installation based on the UVN-2M pumping system (Russia) consisting of a three-position ESA module, which was adapted for operation in vacuum and various gas media, and an PCAE unit. The doping process was carried out in an Ar medium (99.9995%) in the reverse polarity mode (electrode-cathode) with the following processing parameters: voltage 100 V, pulse repetition rate 100 Hz pressure 30 Pa, pulse duration 50 µs, and number of passes 10.

During the PCAE process, the working gas pressure (Ar) was 0.5 Pa; the residual pressure was 2 × 10⁻² Pa; the discharge voltage ranged from 160 to 200 V; and

the voltage and frequency of ignition were 15 kV and 10 Hz, respectively. Before applying the coatings, the substrates were cleaned when a negative bias voltage (2 kV) was applied to them in argon for 5 min.

The morphology and elemental and phase compositions of the electrodes and coatings were determined using scanning electron microscopy (SEM), energy dispersive spectroscopy (EDS) on a Hitachi S-3400N microscope (Japan) with a Noran 7 Thermo attachment, and X-ray diffraction (XRD) on an AXS D8 ADVANCE instrument (Bruker, Germany) using CuK_α-radiation.

Tribological tests to determine the friction coefficient were carried out on a high-temperature tribometer CSM Instruments (Switzerland) according to the rod scheme–drive with an Al₂O₃ ball (6 mm in diameter) at a load of 1 N (for ESA and PCAE samples) and 5 and 10 N (for ESA samples). A WYKO NT 110 optical profiler was used to determine the roughness and study the coating wear paths.

The electrochemical properties of the coatings were evaluated using a three-electrode cell with a VoltaLab 50 potentiostat (Radiometer Analytical, France). The tests were carried out in a solution of 1 N H₂SO₄ using a reference Ag/AgCl electrode and an auxiliary Pt electrode. All potentials were recalculated relative to the standard hydrogen electrode. The corrosion current density was calculated using the Tafel formula.

RESULTS AND DISCUSSION

Structure and Composition of Electrodes and Coatings

SEM images of TiCNiCr and TiCNiCr–Dy₂O₃ electrodes are shown in Fig. 1. It can be seen that they consist of TiC grains (dark areas in micrographs), a solid solution of Ni in Cr (gray areas), and Dy₂O₃ (white areas) in the case of a doped electrode. The grain sizes of titanium carbide for the electrodes reached 12 µm and the particles Dy₂O₃ were around 5 µm.

The microstructure of electrospark coatings, obtained with the use of TiCNiCr and TiCNiCr–Dy₂O₃ electrodes, is shown in Fig. 2. It is seen that it is typical for ESA coatings and has a small number of defects (pores and condensed spray of molten material). The coatings have an identical relief.

Samples obtained using a TiCNiCr electrode have the following composition, at %: 16.0 Ti, 34.0 C, 8.0 Cr, 4.6 Ni, and 37.4 Fe. In the case of using a doped electrode, the coating contains, at %, 17.9 Ti, 25.9 C, 8.3 Cr, 3.1 Ni, 29.4 Fe, 13.0 O, and 2.4 Dy. Dysprosium oxide is distributed along the boundaries of droplets on the coating surface, which can be explained by a lower density Dy₂O₃ when compared with other coating elements. In our previous work [13] it was shown that Eu₂O₃ was located mostly on the border of the substrate-coating. This difference in phase

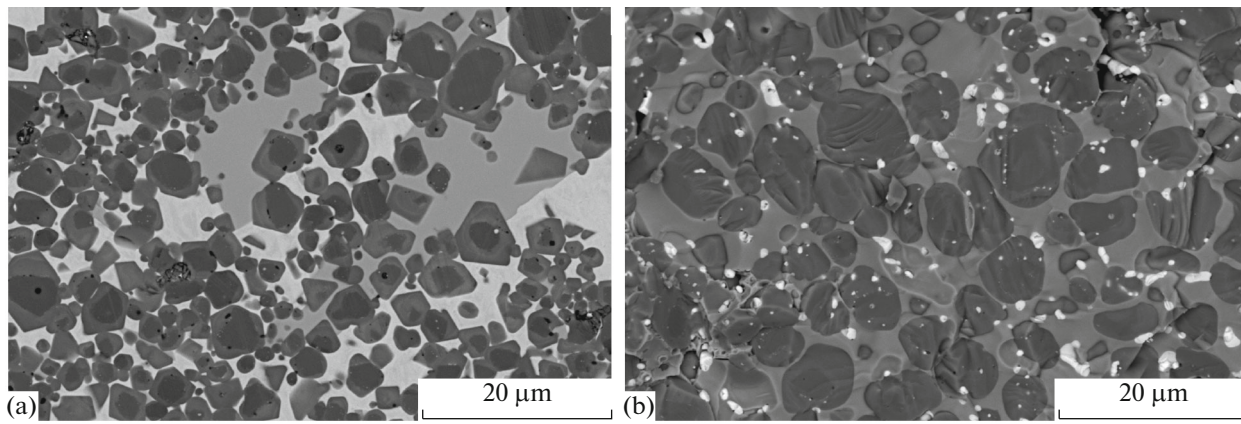


Fig. 1. Electrode structure TiCNiCr (a) and TiCNiCr–Dy₂O₃ (b).

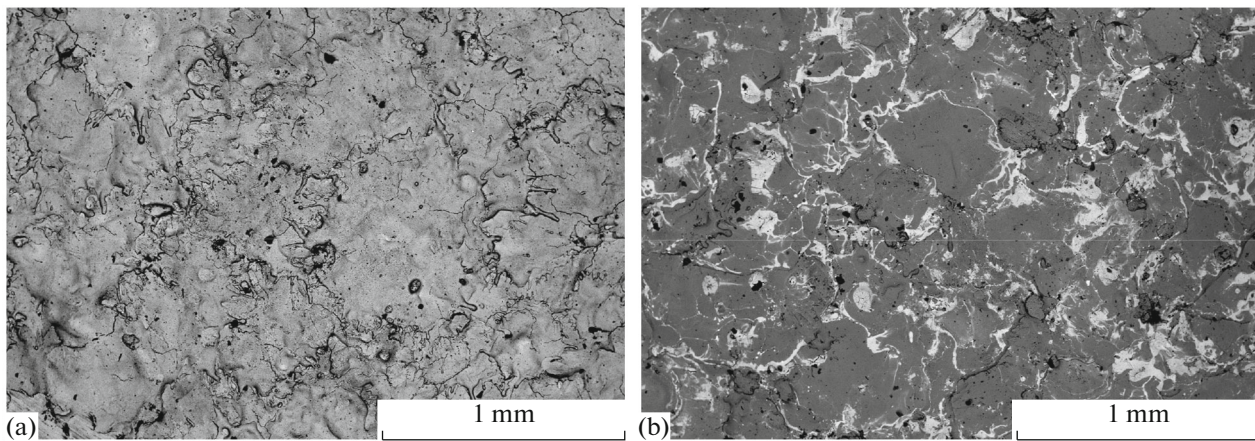


Fig. 2. SEM images of the surface microstructure of electrospray coatings obtained with TiCNiCr electrodes (a) and TiCNiCr–Dy₂O₃ (b).

distribution can be explained by a higher amount of metal components (Ni and Cr) in the TiCNiCr–Dy₂O₃ electrode; during its melting, the material is transferred through the liquid phase. In the case of using an electrode with an Eu₂O₃ additive and with a lower concentration of Ni and Cr, the particles are transported through the solid phase.

Figure 3 shows that the coatings have a fine-grained structure: the minimum TiC grain size was about 30 nm, the maximum was 3 μm, and dysprosium oxide was on the order of 1 μm. An analysis of cross sections showed that ESA coatings consist of dark grains of titanium carbide, gray sections corresponding to a solid solution of Ni and Cr in Fe, and white grains of Dy₂O₃ (in the case of doped coating). The size of the interlayers ranged from 40 nm to 2.5 μm. The TiCNiCr–Dy₂O₃ coating thickness was about 30 μm. The PCAE coating had a uniform structure without pronounced columnar elements. The composition of the upper layer, determined by the EDS method, was as follows, at %: 34.9 Ti, 9.0 C,

22.5 Cr, 18.2 Ni, 8.1 O and 5.9 Dy, and its thickness was 2.2 μm.

The XRD results (Fig. 4) confirm the EDS data for coatings obtained using the base electrode and the electrode with the addition of Dy₂O₃. The peaks corresponding to the (110), (220) and (310) planes belong to the α-Fe phase. For both samples, peaks are observed associated with reflections from the (111), (200), (220), (311), (222), and (400) planes of the fcc phase based on titanium carbide. There are also peaks of a solid solution of nickel and chromium in iron—Fe (NiCr). The X-ray diffraction patterns of coatings obtained using a doped electrode reveal peaks associated with reflection from the (321), (400), (411), and (444) planes of Dy₂O₃.

The crystallite size of titanium carbide, determined from the broadening of the (111) and (200) lines, did not differ for any coatings and amounted to 22 and 18 nm, respectively. The Dy₂O₃ crystallite size was in the range from 6 to 30 nm.

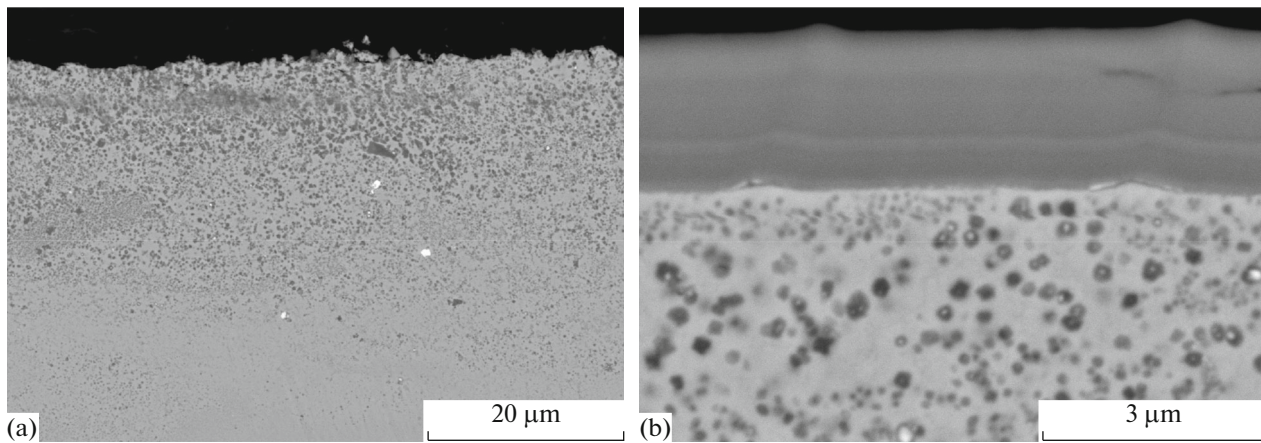


Fig. 3. SEM images of transverse sections of coatings obtained by the ESA method (a) and ESA-PCAE (b) using a TiCNiCr–Dy₂O₃ electrode.

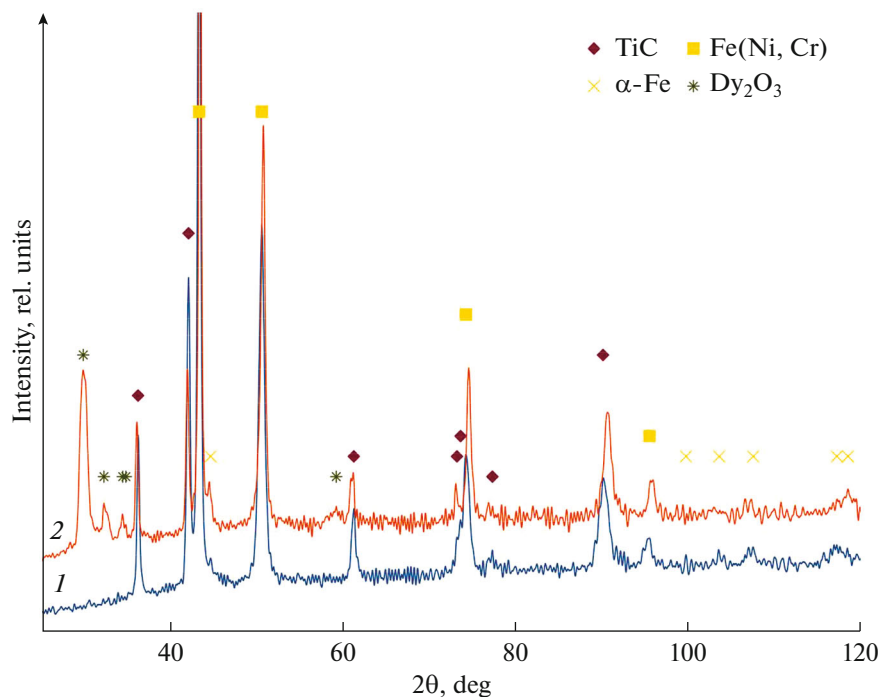


Fig. 4. XRD patterns of coatings obtained using TiCNiCr (1) and TiCNiCr–Dy₂O₃ electrodes (2).

For the coating obtained by PCAE, peaks of the fcc phase based on TiC associated with reflections from the (111) and (200) planes were found. The crystallite size of titanium carbide was about 2 nm.

Tribological Properties of Coatings

According to the results of the tribological tests shown in Figs. 5 and 6, the coefficient of friction (f) of an ESA coating obtained using a TiCNiCr electrode under load $R = 1$ N was stable over distance $l = 0$ –150 m and amounted to 0.18.

At a distance of 150–200 m, the average value of f was 0.25. The Dy₂O₃ spray-coated sample possessed a lower coefficient of friction (0.11) than the underdoped coating, with $R = 1$ N. In the case of a load of 5 N, the value f base coverage in the range from 0 to 100 m gradually increased from 0.13 to 0.27, after which it rose sharply to 0.66. For the sample with Dy₂O₃, the coefficient of friction gradually increased from 0.11 to 0.3 over a distance of 0–150 m, and over the next 50 m it rose to 0.6. At $R = 10$ N, indicator f of the undoped coating for the first 30 m changed from 0.12 to 0.75; wear of the coating was observed after 30 m of the test ($f = 0.7$ –0.8).

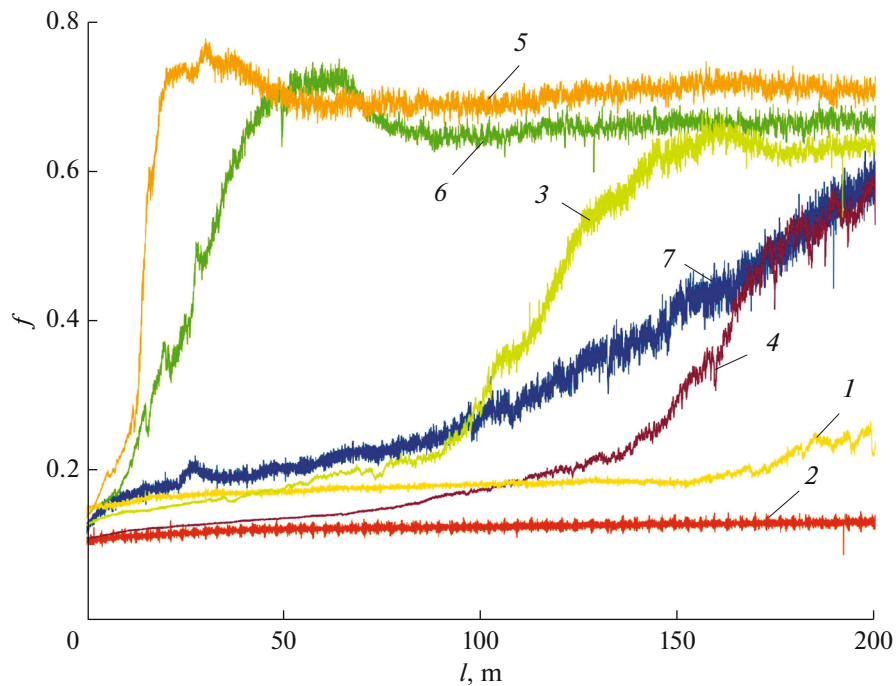


Fig. 5. Plot of the coefficient of friction versus the distance of TiCNiCr coatings at loads of 1 N (1), 5 N (3), and 10 N (5); TiCNiCr–Dy₂O₃ at 1 N (2), 5 N (4), and 10 N (6); and ESA-PCAE coatings at 1 N (7).

When conducting research on coatings obtained using a TiCNiCr–Dy₂O₃ electrode, the value of f at a load of 10 N rapidly increased from 0.13 to 0.73 at a distance of 0–60 m and then, as a result of the action of wear products, it decreased and remained within the range of 0.64–0.67 over the remaining distance. A high coefficient of friction at loads of 5 and 10 N for electrospark coatings with the addition of Dy₂O₃ occurs later (at a distance of 50 and 30 m) in comparison with the base coat, which indicates their higher wear resistance due to the use of a doped electrode. For a multilayer coating with the addition of Dy₂O₃ at $R = 1$ N, a low (at the level of 0.14) coefficient of friction of up to 80 m was observed; however, when it reached a distance of 200 m, it increased to 0.6.

Based on their data, it can be concluded that a single-layer ESA coating has a low coefficient of friction at loads of 1 N, while an upper layer increases it 1.5 times. A multilayer coating exhibits smoother growth of f as a result of the removal of wear products from the contact zone. The wear of the coatings could not be determined due to the high surface roughness: $R_a = 6.0$ – 7.2 μm .

Corrosion Resistance of Coatings

Polarization curves in semilogarithmic coordinates for the substrate, reference sample (X18H10T stainless steel), single-layer coatings, and multilayer coatings are shown in Fig. 7. It can be seen that, at potentials above 1.75 V, the breakdown of the passive film was observed for all samples. Note that the corrosion

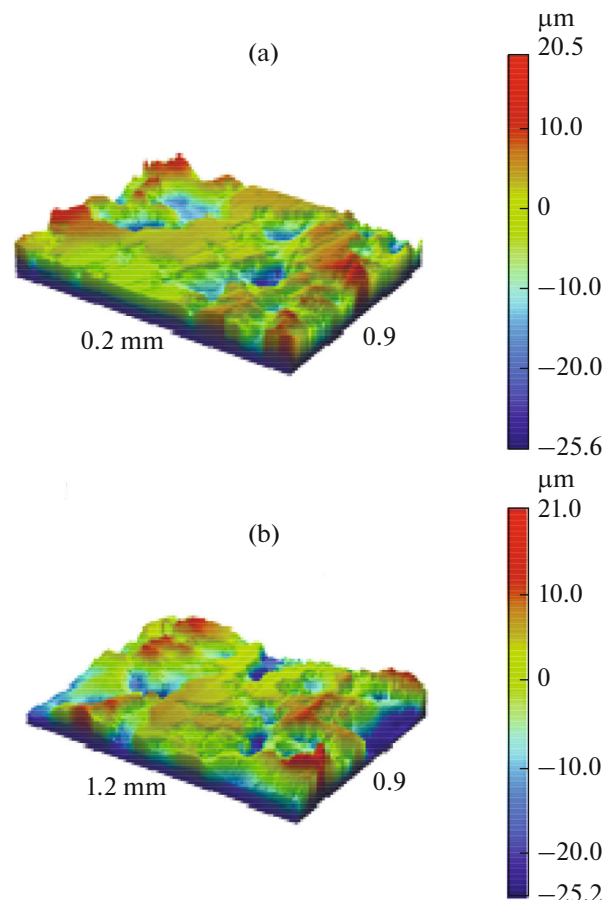


Fig. 6. Paths of wear of the base coating (a) and coatings with the addition of Dy₂O₃ (b) at a load of 10 N.

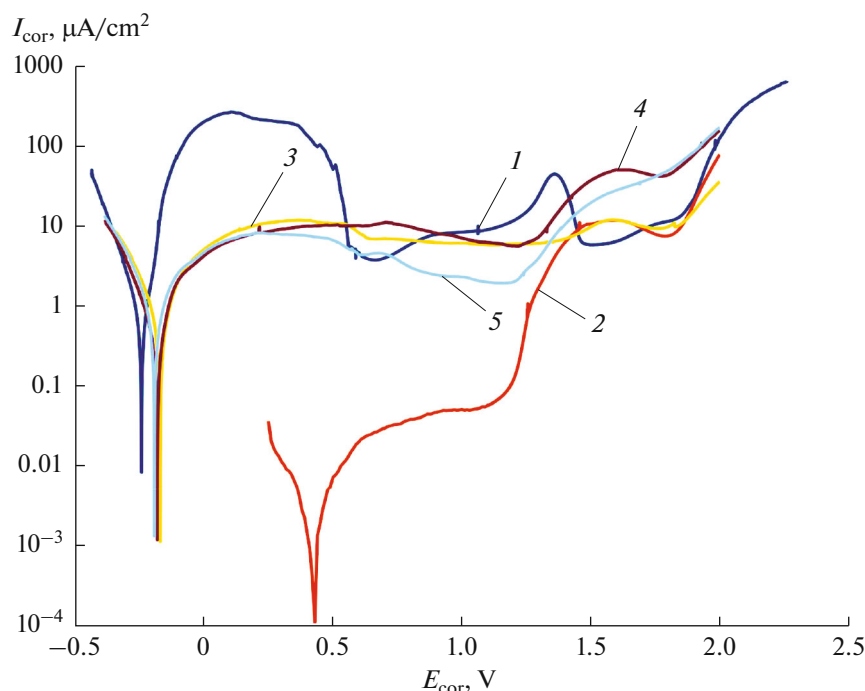


Fig. 7. Polarization curves for substrate 40Cr (1), steel X18H10T (2), ESA coatings deposited using TiCNiCr (3) and TiCNiCr–Dy₂O₃ electrodes (4), and a multilayer coating (5).

potential of all coatings deposited on a steel substrate corresponds to the free corrosion potential of iron (–190 V). This is due to the fact that the electrolyte through cracks and defects of the coating reaches the substrate and the abundant dissolution of its components occurs. ESA coatings using TiCNiCr and TiCNiCr–Dy₂O₃ electrodes had close values of the current density of corrosion $I_{\text{cor}} = 0.20$ and 0.18 mA/cm², respectively (Table 2). All coatings in the 1 N H₂SO₄ solution were in a stable passive state.

The corrosion current density of single-layer coatings is 5.5 times lower than the values obtained for the substrate (1.1 mA/cm²). The deposition of the upper arc layer of TiCNiCr led to an increase in I_{cor} by 30%.

Table 2. Potential and current density of corrosion of alloys and coatings in 1N H₂SO₄

Sample	E_{cor} , mV	I_{cor} , mA/cm ²
Steel 40Cr (substrate)	–235	1.1
Steel X18H10T	+470	0.001
TiCNiCr (ESA)	–168	0.20
TiCNiCr–Dy ₂ O ₃ (ESA)	–178	0.19
TiCNiCr (ESA–PCE)	–195	0.26

For multilayer coatings, $I_{\text{cor}} = 0.26$ mA/cm², which is 4 times lower than that of the substrate. The corrosion potential after the deposition of single-layer and multilayer coatings became more positive and approached the value of E_{cor} for X18H10T stainless steel.

CONCLUSIONS

The ESA method and combined ESA–PCE technology using TiCNiCr and TiCNiCr–Dy₂O₃ electrodes were used to obtain coatings on a steel (grade 40Cr) substrate. They contained a TiC phase, a layer of a solid solution of Ni and Cr in Fe, and Dy₂O₃ (TiCNiCr–Dy₂O₃ electrode). The introduction of dysprosium oxide reduced the coefficient of friction by at least 30% and did not have a noticeable effect on corrosion resistance.

It was established that the deposition of single and multilayer coatings contributes to a decrease in the current density of the corrosion of the substrate by at least 4 times. The resulting coatings can be used to increase the tribological characteristics and corrosion resistance of critical machine parts.

ACKNOWLEDGMENTS

We are grateful to N.V. Shvyndina (MISiS) for help in conducting structural studies of coatings.

FUNDING

This study was supported by the Russian Science Foundation (project no. 15-19-00203-P).

CONFLICT OF INTEREST

The authors declare that they have no conflict of interest.

REFERENCES

- Wang, X., He, X., and Guo, H., Influence of Mo on the microstructure and mechanical properties of TiC-based cermets, *Rare Met.*, 2010, vol. 29, pp. 346–350.
- Levinskii, Yu.V. and Petrov, A.P., Tungsten-free hard alloys based on titanium carbide, *Inorg. Mater.*, 2000, vol. 36, pp. 24–27.
- Rajabi, A., Ghazali, M.J., Syarif, J., and Daud, A.R., Development and application of tool wear: A review of the characterization of TiC-based cermets with different binders, *Chem. Eng. J.*, 2014, vol. 255, pp. 445–452.
- Liu, Z., Tian, J., Li, B., and Zhao, L., Microstructure and mechanical behaviors of in situ TiC particulates reinforced Ni matrix composite, *Mater. Sci. Eng., A*, 2010, vol. 527, pp. 3898–3903.
- Kiryukhantsev-Korneev, Ph.V., Sheveyko, A.N., Shvindina, N.V., Levashov, E.A., and Shtansky, D.V., Comparative study of Ti–C–Ni–Al, Ti–C–Ni–Fe, and Ti–C–Ni–Al/Ti–C–Ni–Fe coatings produced by magnetron sputtering, electro-spark deposition, and a combined two-step process, *Ceram. Int.*, 2018, vol. 44, pp. 7637–7646.
- Andreev, A.V., Litovchenko, I.Y., Korotaev, A.D., and Borisov, D.P., Thermal stability of Ti–C–Ni–Cr and Ti–C–Ni–Cr–Al–Si nanocomposite coatings, *J. Phys.: Conf. Ser.*, 2015, vol. 652, p. 012057.
- Nikolenko, S.V., Verkhoturov, A.D., Syui, N.A., and Kuz'michev, E.N., Influence of electrospark discharge parameters on roughness and microabrasive wear of steel 45 surface after ESA by TiC-based electrodes, *Surf. Eng. Appl. Electrochem.*, 2016, vol. 52, pp. 342–349.
- Levashov, E.A., Malochkin, O.V., Kudryashov, A.E., Gammel, F., and Suchentrunk, R., Effects of nanocrystalline powders additions on the characteristics of combustion process, phase and structure-formation, and properties of SHS alloys on titanium carbide base, *J. Mater. Synth. Process.*, 2002, vol. 10, pp. 231–236.
- Quazi, M.M., Fazal, M.A., Hasee, A.S.M.A., Yusof, F., Masjuki, H.H., and Arslan, A., Effect of rare earth elements and their oxides on tribo-mechanical performance of laser claddings: A review, *J. Rare Earths*, 2016, vol. 34, pp. 549–564.
- Zhu, R., Li, Z., Li, X., and Sun, Q., Microstructure and properties of the low-power-laser clad coatings on magnesium alloy with different amount of rare earth addition, *Appl. Surf. Sci.*, 2015, vol. 353, pp. 405–413.
- Kiryukhantsev-Korneev, F.V., Sytchenko, A.D., Kudryashov, A.E., and Levashov, E.A., Protective coatings produced by electro-spark deposition with TiCr–(Eu₂O₃) electrodes, *CIS Iron Steel Rev.*, 2018, vol. 16, pp. 57–62.
- Kiryukhantsev-Korneev, Ph., Sytchenko, A., Sheveyko, A., and Vorotilo, S., Deposited by pulsed cathodic arc evaporation in Ar, N₂, and C₂H₄ environments using the TiC–NiCr–Eu₂O₃ cathode, *Coatings*, 2019, vol. 9, pp. 230–243.
- Kiryukhantsev-Korneev, Ph.V., Sytchenko, A.D., and Levashov, E.A., Comparative study of electrospark alloying coatings formed using TiC–NiCr and TiC–NiCr–Eu₂O₃ electrodes, *Russ. J. Non-Ferrous Met.*, 2019, vol. 60, no. 6, pp. 662–672.
- Kiryukhantsev-Korneev, Ph.V., Sheveyko, A.N., Kuptsov, K.A., Novikov, A.V., and Shtansky, D.V., Ti–Cr–B–N coatings prepared by pulsed cathodic-arc evaporation of ceramic TiCrB target produced by SHS, *Prot. Met. Phys. Chem. Surf.*, 2013, vol. 49, pp. 677–681.
- Dong, X., Cheng, X.L., Zhang, X.F., Sui, L.L., Xu, Y.M., and Gao, S., A novel coral-shaped Dy₂O₃ gas sensor for high sensitivity NH₃ detection at room temperature, *Sens. Actuators, B*, 2018, vol. 255, pp. 1308–1315.
- Wei, C.C., Transparent ceramics for lighting, *J. Eur. Ceram. Soc.*, 2009, vol. 29, pp. 237–244.
- Ramay, S.M. and Saleem, M., Magnetron sputtered Dy₂O₃ with chromium and copper contents for antireflective thin films with enhanced absorption, *J. Rare Earths*, 2019, vol. 37, pp. 989–994.
- Liu, X. and Huang, W., Preparation and tribological performance of electrodeposited Ni–TiB₂–Dy₂O₃ composite coatings, *J. Rare Earths*, 2009, vol. 27, pp. 480–485.